



Short communication

Cathode properties of metal trifluorides in Li and Na secondary batteries<sup>☆</sup>Manabu Nishijima<sup>a</sup>, Irina D. Gocheva<sup>a</sup>, Shigeto Okada<sup>a,\*</sup>, Takayuki Doi<sup>a</sup>, Jun-ichi Yamaki<sup>a</sup>, Tetsuaki Nishida<sup>b</sup><sup>a</sup> Institute of Materials Chemistry and Engineering, Kyushu University, 6-1 Kasuga Koen, Kasuga-shi 816-8580, Japan<sup>b</sup> School of Humanity-Oriented Science and Engineering, Kinki University, Kayanomori, Iizuka 820-8555, Japan

## ARTICLE INFO

## Article history:

Received 16 August 2008

Received in revised form 3 November 2008

Accepted 19 January 2009

Available online 30 January 2009

## Keywords:

Metal trifluoride

Perovskite

Na secondary battery

## ABSTRACT

Fluorine compounds have high discharge voltage due to its highly ionic metal-ligand bonds. In them, perovskite-type metal trifluorides with corner sharing matrix have large bottlenecks of diffusion pathways for intercalants. Iron trifluoride composites (FeF<sub>3</sub>-C) prepared by planetary ball milling with carbon showed reversible charge/discharge behavior not only for Li, but also for Na anodes. X-ray diffraction and <sup>57</sup>Fe Mössbauer spectroscopy were applied to characterize the electrochemical properties of FeF<sub>3</sub> vs. Li and Na anodes. The cathode performances of the other commercially available transition metal trifluorides such as MF<sub>3</sub> (M = Ti, V, Mn, Co) have been also investigated.

© 2009 Elsevier B.V. All rights reserved.

## 1. Introduction

Due to the high electronegativity of fluorine, fluoride cathodes take a prominent place for energy conversion and storage, in comparison with sulfide and oxide cathodes [1,2]. In these fluoride cathodes, perovskite-type transition metal trifluorides, MF<sub>3</sub>, are attractive as not only high-voltage cathode, but also large-capacity cathode. Nowadays the phospho-olivine LiFePO<sub>4</sub> is considered as the most promising rare-metal free cathode for next generation large scale Li-ion batteries for electric vehicle, because of its large theoretical capacity, low material cost, low-toxicity and safety [3,4]. However, the theoretical specific capacity of rare-metal free FeF<sub>3</sub> is 237 mAh g<sup>-1</sup>, which is beyond that of LiFePO<sub>4</sub> (170 mAh g<sup>-1</sup>). In addition, the chemical composition includes no oxygen that becomes the cause of exothermic heat generation.

The cathode performance of the first report [5] about the MF<sub>3</sub> (M = Fe, V, Ti, Mn and Co) was not so remarkable, because the reported reversible capacity of FeF<sub>3</sub> was only 80 mAh g<sup>-1</sup> which was 34% of the theoretical capacity corresponding to Fe<sup>3+</sup>/Fe<sup>2+</sup> redox reaction and the discharge voltage was lower than that of LiFePO<sub>4</sub>. Generally, ionic character of the metal/halogen bond brings metal trifluorides to the poor electronic conductivity with wide energy gap. However, much success has been achieved through mechanical milling with carbon and good reversible behavior of approximately

200 mAh g<sup>-1</sup> in 3 V region has been disclosed for the FeF<sub>3</sub>-C composite cathode [6]. In addition, transition metal fluorides such as FeF<sub>3</sub>, TiF<sub>3</sub> and VF<sub>3</sub> exhibited reversible conversion reaction with 2–3 Li per mole at lower voltage [7–9].

Meanwhile Na-ion battery has drawn our attention as low cost and low environmental impact power device in recent years, because of the good economical efficiency, rich resources and low toxic nature [10–14]. However, the standard electrode potential of Na (–2.71 V vs. SHE) is not low as that of Li (–3.05 V vs. SHE). Furthermore, Na is air sensitive and the ionic volume is almost 2 times larger than that of Li. Therefore, published papers about cathode active materials for Na anode has been restricted within narrow material groups such as two-dimensional layered compounds with van der Waals gap (ex. TiS<sub>2</sub> [15]) and three-dimensional compounds with corner sharing matrix (ex. FeS<sub>2</sub> [16]).

The aim of this paper is to investigate the reversible behavior of transition metal trifluorides for Na intercalation as well to confirm results already known vs. Li. Most of the MF<sub>3</sub> structures are related to the ReO<sub>3</sub> perovskite structure with R3-c [5,14]. An ideal perovskite structure with cubic symmetry consists of a three-dimensional framework of corner-sharing BX<sub>6</sub> octahedron. We expect that the A-site surrounded by 12 equidistant fluorines in perovskite matrix must be suitable cavity not only for Li but also for Na intercalation.

In this paper, the electrochemical properties of FeF<sub>3</sub> cathodes for Li and Na cells were investigated. Iron valence changes in FeF<sub>3</sub> vs. Li or Na anodes were investigated by <sup>57</sup>Fe Mössbauer spectroscopy. The cathode properties of the other transition metal trifluorides (M = V, Ti, Mn, Co) have been also examined.

<sup>☆</sup> Paper presented at ICFMD 2008, Kuala Lumpur, Malaysia.

\* Corresponding author. Tel.: +81 92 583 7841; fax: +81 92 583 7841.

E-mail address: [s-okada@cm.kyushu-u.ac.jp](mailto:s-okada@cm.kyushu-u.ac.jp) (S. Okada).

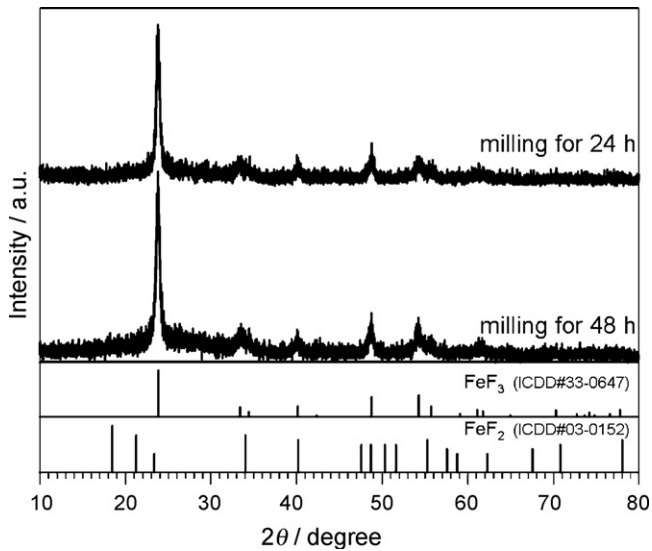


**Fig. 1.** XRD profiles of  $\text{FeF}_3\text{-C}$  composite cathode after 24 h and 48 h milling treatment.

## 2. Experimental

Commercially available  $\text{FeF}_3$ ,  $\text{VF}_3$ ,  $\text{TiF}_3$ ,  $\text{MnF}_3$  (Soekawa Chemical Co.) and  $\text{CoF}_3$  (Strem Chemicals Inc.) were used in this research. All of them were analytical grade. Powder reagents were grinded by using the planetary ball mill at 200 rpm with 25 wt% acetylene black (AB; Denki Kagaku Kogyo) for various milling time (1–48 h) in Ar atmosphere.  $\text{MF}_3\text{-C}$  composite has been mixed with 5 wt% polytetrafluoroethylene (Daikin Industries, Ltd.). Cathode pellets were punched in the form of disks (ca. 30 mg in weight and 10 mm in diameter) in an Ar-filled glove box and dried at 100 °C under vacuum overnight.

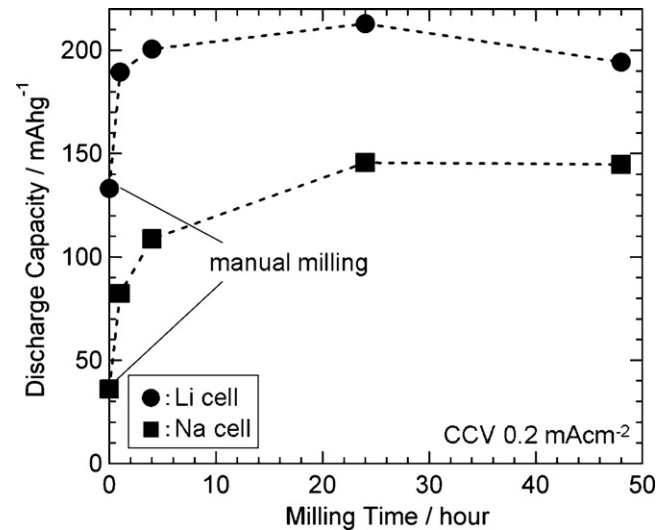


**Fig. 2.** First discharge capacities of  $\text{FeF}_3$  vs. Li/Na anode as function of milling time with AB.

The 2032 coin-type cells were assembled with microporous polypropylene separator (Celgard LLC) in an Ar-filled glove box. 1 mol  $\text{dm}^{-3}$   $\text{NaClO}_4/\text{PC}$  (Tomiya Pure Chemical Industries, Ltd.) and 1 mol  $\text{dm}^{-3}$   $\text{LiPF}_6/\text{EC}+\text{DMC}$  (1:1 in volume, Tomiyama Pure Chemical Industries, Ltd.) were used as nonaqueous electrolyte in Na (Sigma–Aldrich) and Li (Honjo Metal Co., Ltd.) cell, respectively. Galvanostatic cycling was performed at a rate of 0.2 mA  $\text{cm}^{-2}$ . The voltage range was controlled between 1.5 V and 4.0 V for Na anode and 2.0–4.5 V for Li anode, respectively (NAGANO BTS-2004W).

Structural changes of  $\text{FeF}_3\text{-C}$  by mechanical milling with AB were analyzed by X-ray diffraction (XRD; Rigaku RINT2100HLR/PC) with  $\text{Cu-K}\alpha$  radiation. The changes of iron oxidation state during cycling were measured by  $^{57}\text{Fe}$  Mössbauer spectroscopy (Labora-

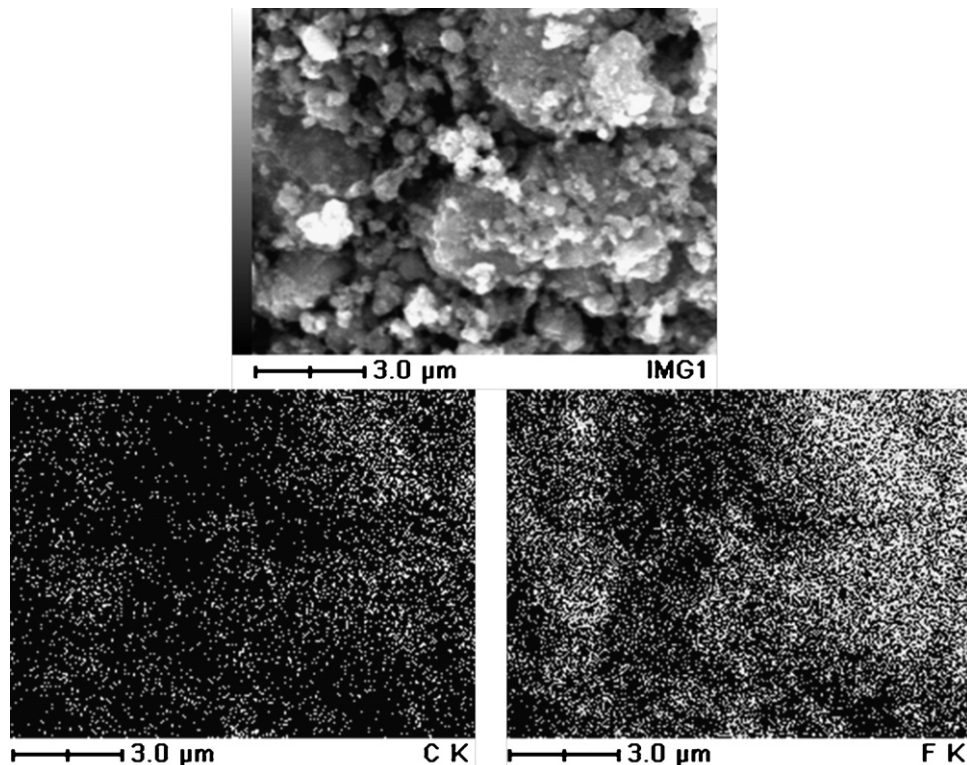


**Fig. 3.** SEM and EDS mapping images of  $\text{FeF}_3$  after 24 h milling with 25 wt% AB.

tory Equipment Co., Ltd.). Dynamic light scattering particle size analyzer (HORIBA LB-500X) was used to measure particle size distribution.

### 3. Results and discussion

To optimize the milling conditions,  $\text{FeF}_3$  powder sample has been grinded with 25 wt% acetylene black for various milling time. During the ball milling treatment, any traces of fluorine release from  $\text{FeF}_3$  were not observed. The basic perovskite structure of  $\text{FeF}_3$  was maintained even after prolonged grinding to 48 h with carbon without reduction of the  $\text{Fe}^{3+}$  to  $\text{Fe}^{2+}$  as shown in Fig. 1. According to Fig. 2, at least several hours milling is needed for  $\text{FeF}_3$ -C composite cathode to obtain enough cathode capacity vs. Li and Na anode. After 24 h milling, the uniform distribution of the carbon black on the  $\text{FeF}_3$  particles has been observed on SEM and EDS mapping images (Fig. 3).

The charge/discharge profiles of  $\text{FeF}_3$ -C composite cathode vs. Li and Na anode are shown in Fig. 4. The initial discharge capacity of  $\text{FeF}_3$ -C/Li cell increases from  $130 \text{ mAh g}^{-1}$  to  $210 \text{ mAh g}^{-1}$  by means of carbon coating treatment, which is consistent with the results reported by Badway [6]. However, prolongation of the milling treatment more than 24 h may not bring additional positive effect on the discharge capacity. The mean particle size of 24 h mechanical milling sample with carbon was  $3.3 \mu\text{m}$ . The new information obtained from this experiment is that carbon coated  $\text{FeF}_3$  composite can work as cathode vs. Na anode with discharge capacity of  $145 \text{ mAh g}^{-1}$ , corresponding to 61% of theoretical value. However, the irreversible capacity of the Na cell is larger than that of Li cell. The reason of the irreversible capacity is the larger discharge/charge overpotential caused by slower intercalation/deintercalation kinetics of larger Na cation and lower cut off voltage for Na cell to avoid electrolyte decomposition and side reactions.

To estimate the equilibrium potential instantly, QOCV profiles of  $\text{FeF}_3$  were measured (Fig. 5). The Li/Na contents in the cathode pellet were calculated by chronometric capacity. Na cell shows slight sloped discharge/charge profile with large polarization, in contrast to flat voltage plateau with 3.3 V vs. Li/Li<sup>+</sup> observed in Li cell.

Rate capability of  $\text{FeF}_3$ -C was studied with various current densities from  $0.1 \text{ mA cm}^{-2}$  to  $5.0 \text{ mA cm}^{-2}$  (Fig. 6). Although the discharge capacity of Li cell maintains  $150 \text{ mAh g}^{-1}$  even at more than  $2 \text{ mA cm}^{-2}$ , the large capacity more than  $150 \text{ mAh g}^{-1}$  is restricted at  $0.1 \text{ mA cm}^{-2}$  or the less in the case of Na cell. On the other hand, Fig. 7 shows the cyclability of  $\text{FeF}_3$ -C with various

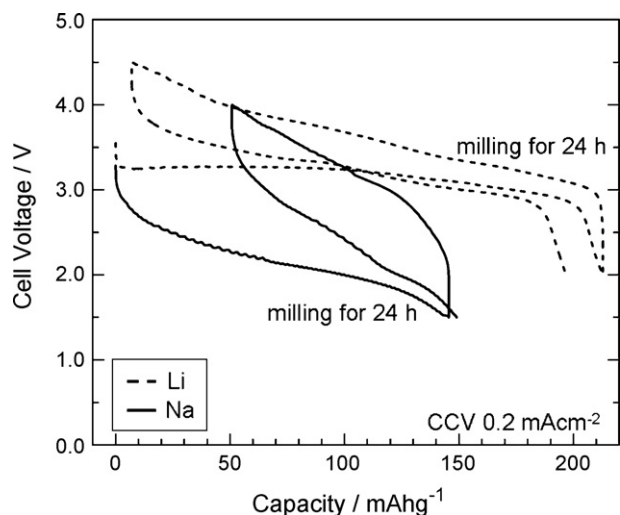


Fig. 4. First and second discharge/charge profiles of  $\text{FeF}_3$ -C vs. Li/Na anode.

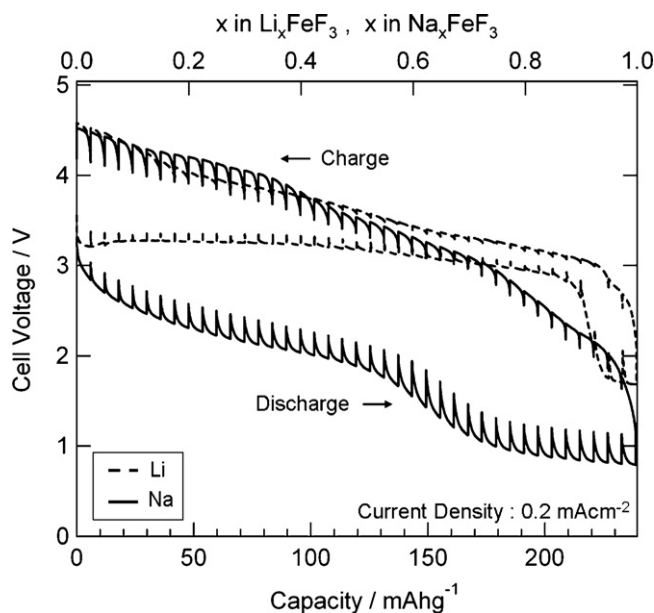


Fig. 5. Quasi open-circuit voltages of  $\text{FeF}_3$ -C vs. Li/Na anode.

milling times in the Na and Li cell. The distinct enhancement of the rechargeable capacity by milling with carbon was observed in both Na and Li cells. This positive effect on the rate capability and cyclability suggests that coated carbon on the  $\text{FeF}_3$  surface enhances the conductivity and suppresses the solubility of ionic metal trifluoride in electrolyte.

Changes of oxidation state of iron during the reduction (Li/Na intercalation) or oxidation (Li/Na deintercalation) were detected by  $^{57}\text{Fe}$  Mössbauer spectra of  $\text{FeF}_3$  (Fig. 8). Under the magnetic transition temperature (363 K), broad line spectrum of initial sample shows two well-defined patterns corresponding to  $\text{FeF}_3$ -sextet and remaining amorphous (doublet) due to the superparamagnetism of ultra fine grains. The sextet for  $\text{FeF}_3$  at a low temperature also shows an isomer shift  $\text{IS} = 0.49 \text{ mm s}^{-1}$  which indicates that iron in  $\text{FeF}_3$  is in  $\text{Fe}^{3+}$  valence state where the high-spin  $\text{Fe}^{3+}$  contains 37% well crystalline component. The partial amorphization is considered as a result of 24 h ball milling procedure applied. During reduction

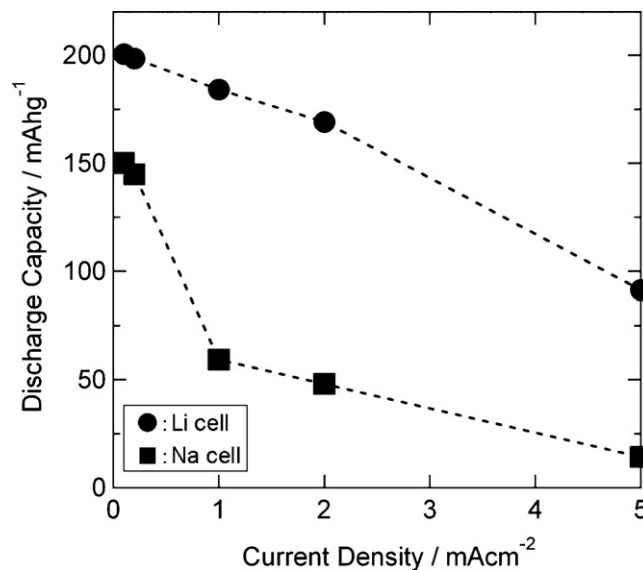


Fig. 6. Discharge rate capability of  $\text{FeF}_3$ -C vs. Li or Na anode. The voltage range was between 1.5–4.0 V (Na cell) and 2.0–4.5 V (Li cell), respectively.

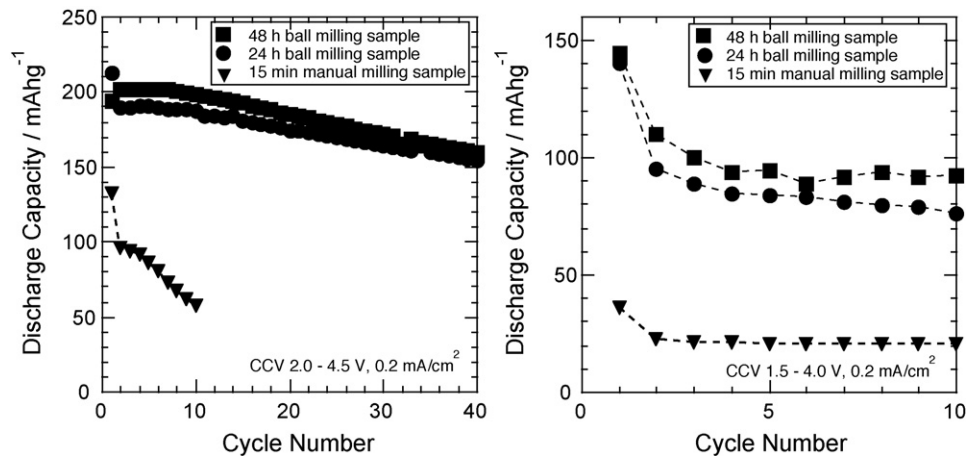


Fig. 7. Cyclability for  $\text{FeF}_3\text{-C}$  with various milling time vs. Li/Na anode.

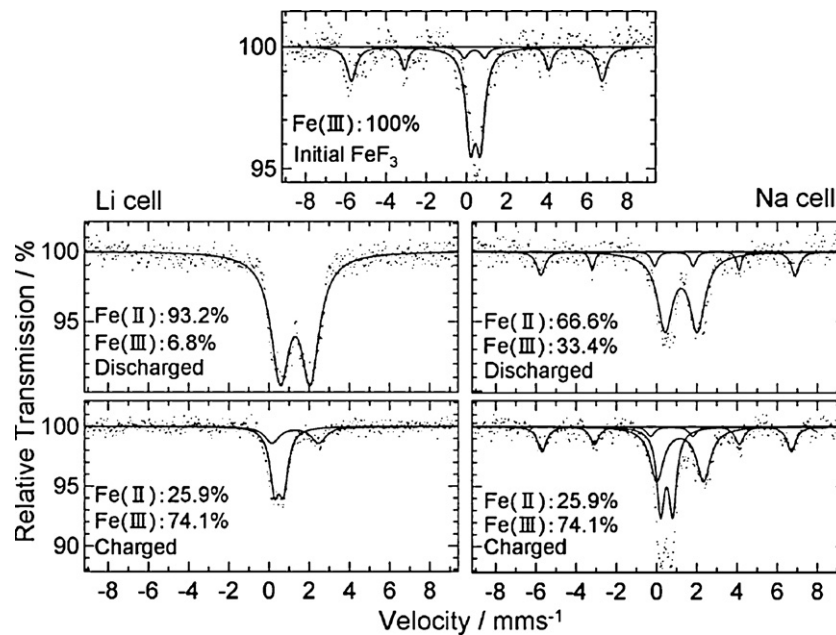


Fig. 8.  $^{57}\text{Fe}$  Mössbauer spectra of  $\text{FeF}_3\text{-C}$  cathode pellets after Li/Na intercalation/deintercalation process.

process in Li cell, 93% of high-spin  $\text{Fe}^{3+}$  changes to high-spin  $\text{Fe}^{2+}$ . It could be attributed to the additional trend of amorphization in depends of depth of Li intercalation. The presence of phase with lower crystallinity was also confirmed by the XRD patterns. In case of Na intercalation only 67% of  $\text{Fe}^{3+}$  changes to  $\text{Fe}^{2+}$ . This detected  $\text{Fe}^{3+}$  ratio at discharged state suggests insufficient intercalation of the large sized Na-ion into  $\text{FeF}_3$  matrix and it quantitatively agrees with the capacity utilization value, 0.63 ( $=150/237$ ) in Fig. 4. Oxidation process recovers 74%  $\text{Fe}^{2+}$  to high-spin  $\text{Fe}^{3+}$  in both cells. It suggests the reversible  $\text{Fe}^{3+}/\text{Fe}^{2+}$  redox reaction corresponding to Li and Na intercalation/deintercalation.

We examined the cathode performance of the other  $\text{MF}_3$  series such as  $\text{VF}_3$ ,  $\text{TiF}_3$ ,  $\text{MnF}_3$  and  $\text{CoF}_3$ , following the above procedure. Concerning the order of redox voltages vs. Li for redox couples,  $\text{Mn}^{3+}/\text{Mn}^{2+}$  (4.22 V) >  $\text{Fe}^{3+}/\text{Fe}^{2+}$  (3.49 V) >  $\text{V}^{3+}/\text{V}^{2+}$  (2.46 V), obtained lower average voltage of  $\text{VF}_3$  are not surprising (Fig. 9). The difference of those mean voltages between  $\text{FeF}_3$  (Fig. 2) and  $\text{VF}_3$  (Fig. 9) was almost 1 V in Li cell and it is same to the standard electrode potential discrepancy between  $\text{Fe}^{3+}/\text{Fe}^{2+}$  (3.49 V) and  $\text{V}^{3+}/\text{V}^{2+}$  (2.46 V). So, it suggests that the charge/discharge process of  $\text{VF}_3$  is the reversible intercalation reaction just as  $\text{FeF}_3$ .

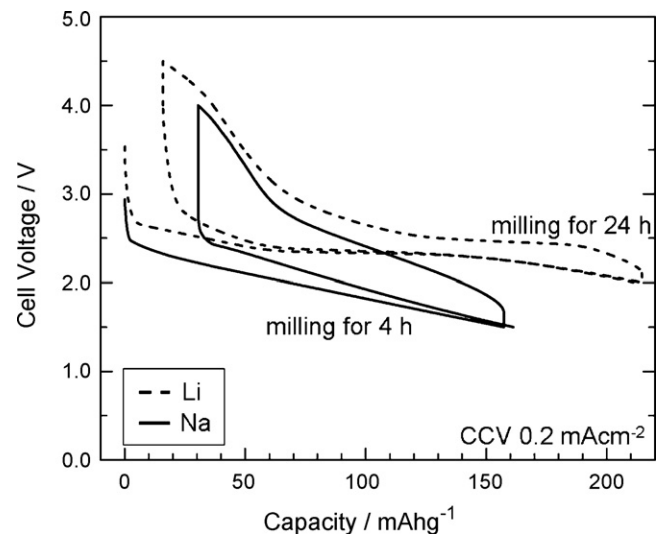


Fig. 9. First and second discharge/charge profiles of  $\text{VF}_3\text{-C}$  vs. Li/Na anode.

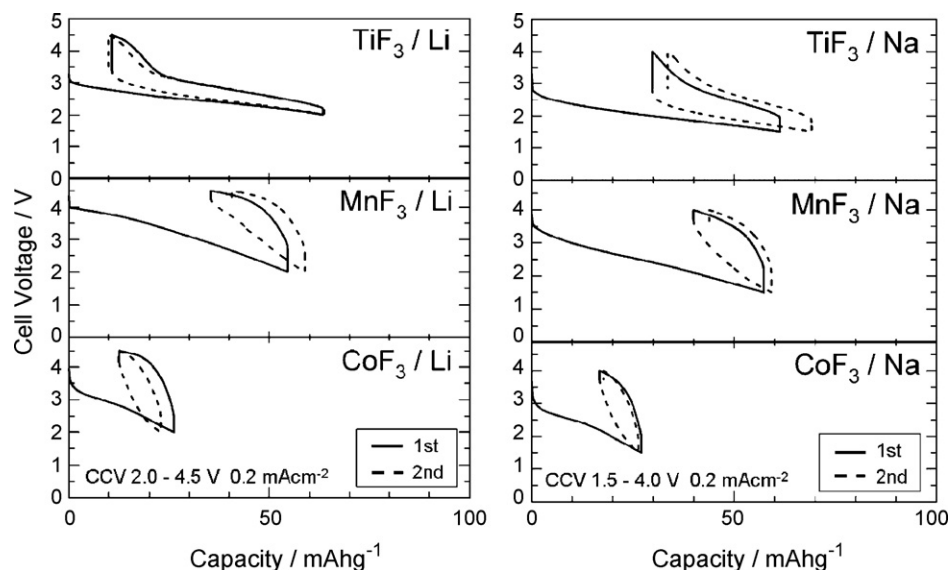


Fig. 10. First and second discharge/charge profiles of  $\text{TiF}_3$ ,  $\text{CoF}_3$  and  $\text{MnF}_3$  carbon composites vs. Li/Na anode.

However in case of Na cell, average discharge voltage of sloped region was 2.1 V and it is almost same to that of  $\text{FeF}_3$ , because of the low polarization of  $\text{VF}_3$ . Fig. 10 shows the charge/discharge profiles of  $\text{TiF}_3$ ,  $\text{CoF}_3$  and  $\text{MnF}_3$  (mechanical milling with AB for 1 h) in Li and Na cells.  $\text{TiF}_3$  and  $\text{CoF}_3$  have the same layer structures R3-c. In contrast,  $\text{MnF}_3$  is distorted and the unit lattice is not rhombohedral but monoclinic by the Jahn-Teller effect of  $\text{Mn}^{3+}$ . According to the estimation from the standard electrode potential of  $\text{M}^{3+}/\text{M}^{2+}$  redox,  $\text{TiF}_3$  must show the mean voltage at 2.1 V,  $\text{MnF}_3$  has at 4.0 V, and  $\text{CoF}_3$  has at 4.4 V in Li cell, respectively. Therefore the small rechargeable capacities with low discharge voltage of  $\text{MnF}_3$  and  $\text{CoF}_3$  in Fig. 10 are probably caused by the insufficient charge cutoff voltage to avoid the electrolyte decomposition.

#### 4. Conclusions

We proposed perovskite-type metal trifluoride with corner sharing matrix is a new big cathode material group not only for Li, but also for Na.  $\text{FeF}_3$  milled for 24 h with carbon exhibited the mean discharge voltage of 2.2 V and the reversible capacity of  $100 \text{ mAh g}^{-1}$  in Na cell. Besides it shows also the 1st discharge capacity of over  $200 \text{ mAh g}^{-1}$  in Li cell. Reversible  $\text{Fe}^{3+}/\text{Fe}^{2+}$  redox reaction in  $\text{FeF}_3$  corresponding to Li and Na intercalation/deintercalation could be confirmed by  $^{57}\text{Fe}$  Mössbauer spectra. The rechargeable capacity in Li cell is beyond the theoretical capacity of olivine-type  $\text{LiFePO}_4$  and the  $620 \text{ mWh g}^{-1}$  ( $=200 \text{ mAh g}^{-1} \times 3.1 \text{ V}$ ) is the highest energy density value in iron-based rare-metal free cathodes. Moreover, it is noteworthy that perovskite-type metal trifluorides are also promis-

ing in the standpoint of the safety, because there is no risk to release any oxygen in cell.

#### Acknowledgement

The present work was financially supported by Li-EAD project of New Energy and Industrial Technology Development Organization, Japan.

#### References

- [1] Y. Koyama, I. Tanaka, H. Adachi, J. Electrochem. Soc. 147 (2000) 3633.
- [2] S. Okada, M. Ueno, Y. Uebou, J. Yamaki, J. Power Sources 146 (2005) 565.
- [3] A.K. Padhi, K.S. Nanjundaswamy, J.B. Goodenough, J. Electrochem. Soc. 144 (1997) 1188.
- [4] A.K. Padhi, K.S. Nanjundaswamy, C. Masquelier, S. Okada, J.B. Goodenough, J. Electrochem. Soc. 144 (1997) 1609.
- [5] H. Arai, S. Okada, Y. Sakurai, J. Yamaki, J. Power Sources 68 (1997) 716.
- [6] F. Badway, N. Pereira, F. Cosandey, G.G. Amatucci, J. Electrochem. Soc. 150 (2003) A1209.
- [7] F. Badway, F. Cosandey, N. Pereira, G.G. Amatucci, J. Electrochem. Soc. 150 (2003) A1318.
- [8] H. Li, P. Balaya, J. Maier, J. Electrochem. Soc. 151 (2004) A1878–A1885.
- [9] H. Li, G. Richter, J. Maier, Adv. Mater. 15 (2003) 736.
- [10] S. Bach, M. Millet, J.P. Pereira-Ramos, L. Sanchez, P. Lavela, J.L. Tirado, Electrochem. Solid-State Lett. 2 (11) (1999) 545.
- [11] Y. Uebou, S. Okada, J. Yamaki, J. Power Sources 115 (2003) 119.
- [12] J. Barker, M.Y. Saidi, J.L. Swoyer, Electrochem. Solid-State Lett. 6 (2003) A1.
- [13] T. Shiratsuchi, S. Okada, J. Yamaki, T. Nishida, J. Power Sources 159 (2006) 268.
- [14] H. Zhuo, X. Wang, A. Tang, Z. Liu, S. Gamboa, P.J. Sebastian, J. Power Sources 160 (2006) 698.
- [15] M.S. Whittingham, Prog. Solid State Chem. 12 (1978) 41.
- [16] T.B. Kim, J.W. Choi, H.S. Ryu, G.B. Cho, K.W. Kim, J.H. Ahn, K.K. Cho, H.J. Ahn, J. Power Sources 174 (2007) 1275.